Applied Energy 183 (2016) 358–368

Contents lists available at ScienceDirect

Applied Energy

journal homepage: www.elsevier.com/locate/apenergy

Electrochemical performance of a short tubular solid oxide fuel cell stack at intermediate temperatures

Navjot Kaur Sandhu [a], Amir Reza Hanifi [a,*], Andrew Woldnik [a], Taghi Amiri [a], Thomas H. Etsell [a], Jingli Luo [a], Partha Sarkar [b]

[a] Department of Chemical & Materials Engineering, University of Alberta, Edmonton, Alberta T6G 1H9, Canada
[b] Alberta Innovates - Technology Futures, Edmonton, Alberta T6N 1E4, Canada

HIGHLIGHTS

- The single cells fabricated for the stack show similar power performances.
- Stack power output in series, parallel and their mixed arrangements was similar.
- Using mixed parallel-series configurations can offer a suitable current or voltage.
- Mixed parallel-series configurations can be fixed in case any fuel cell fails.
- A damaged cell can be replaced in a module not to damage the overall performance.

ARTICLE INFO

Article history:
Received 12 February 2016
Received in revised form 27 August 2016
Accepted 29 August 2016

Keywords:
Micro-tubular
SOFC
Ni-YSZ anode
Stack

ABSTRACT

A short stack composed of six micro-tubular fuel cells was fabricated in order to study its electrochemical performance under different electrical connection configurations (parallel, series and parallel-series) at intermediate temperatures. Two cells were in the Ni-YSZ/YSZ/Pr_2NiO_4-YSZ system and four were in the Ni-YSZ/YSZ/Nd_2NiO_4-YSZ configuration, of which one failed following testing at 600 °C. Overall, individual cells had similar performance delivering 202, 302 and 340 mW/cm^2 at 600, 650 and 700 °C, respectively. The stack delivered a maximum of 7.40, 10.32 and 11.56 W at these temperatures. No significant differences were found among different arrangements. However, as expected, the stack performance was most affected by the malfunctioning cell under a series arrangement at 600 °C. Since the parallel-series configuration delivers an intermediate voltage and current and similar power to the parallel or series connections, it can be more suitable for stack assembly. Such an arrangement also offers the possibility of replacement of a stack module in case a cell fails in that module during operation. A repairable fuel cell stack eliminates the negative economic impacts caused by a malfunctioning cell which, in extreme cases, can lead to the complete loss of the valuable energy conversion device.

1. Introduction

Fuel cell technology is one of the cleanest and most efficient techniques for converting the chemical energy of fuels into electricity [1]. The solid oxide fuel cell (SOFC) or in other words a ceramic fuel cell is a widely investigated device by researchers across the world to eliminate the environmental pollution caused by fossil fuels. The potential market competitiveness of SOFCs arises from: efficiency, flexibility in choice of fuel gas (hydrogen, hydrocarbons), solid and modular construction that has no moving parts, high operating temperature (produces high quality heat as a by-product which can be used for cogeneration), no precious metals involved in fabrication and a potential long life expectancy of more than 40,000–80,000 h [2,3].

The two main fuel cell designs are planar and tubular configurations. Despite the lower power density of tubular fuel cells compared with the planar design, they are preferred since tubular fuel cells require less sealing, show superior thermo-mechanical properties, withstand more thermal cycles and require less start up/shut down time [4–6]. Micro-tubular SOFCs (μt-SOFCs) have a diameter of less than 5 mm which due to their small diameter show a high power density (power density is proportional to the reciprocal tube diameter) and rapid start-up and cool-down time. The micro-tubular design has been seriously considered for portable applications such as cell phone where planar cells cannot be

* Corresponding author.
E-mail address: hanifi@ualberta.ca (A.R. Hanifi).

http://dx.doi.org/10.1016/j.apenergy.2016.08.179
0306-2619/

used [7–9]. A great example of high thermal shock resistance of tubular fuel cells is shown by Du et al. [10]. They fabricated a tubular stack which could withstand more than 50 thermal cycles when single cells were heated at a rate of 550 °C/min to the operating temperature.

The power generated by a single tubular fuel cell is too small for many applications, which necessitates investigation into the design and fabrication of fuel cell stacks for commercial adoption of SOFC technology. Fuel cell stacks have diverse applications such as stationary power generation and in the transportation industry, as shown in Fig. 1. Micro-tubular SOFCs with power output of 1–100 W are being developed by eZelleron for application in portable devices. Ultra Electronics-USSI designs tubular SOFC stacks for back up and portable power for use in oil and gas pipelines and remote sensors as well as for military applications. For instance, the D350 is a compact 350 W SOFC generator for application in expeditionary activities and remote battery charging. Fuel cell stacks producing 10 kW and above are appropriate for stationary applications, while 1–5 kW range stacks can be used for both mobile and stationary (mainly residential) applications. Stacks in the range of 100–500 kW are suitable for distributed power generation, such as Bloom Energy's 400 kW installation on Google's main campus in Mountain View, California.

In the early 1990S, Singhal and Kendall fabricated thin (100–200 μm) YSZ electrolyte supports for application in μt-SOFCs [11]. Following that, Alston et al. [12] from Kendall's research group designed one of the first μt-SOFC stacks, which consisted of 1000 zirconia electrolyte cells assembled into racks of 40 cells. The racks were connected in series, with parallel arrangement of tubes within each rack. The fuel cells were able to withstand 200 °C/min temperature rise, but delivered low power of 0.082 W/cm^2 at 850 °C due to the high ohmic resistance of the electrolyte support. Since then different research groups have attempted to develop different types of anode supported tubular fuel cells stacks. For instance, Lee et al. [5] developed a 700 W anode supported micro-tubular SOFC stack by stacking 36 fuel cells (each 20 cm long) arranged into bundles (of six) which formed a modular type stack. The stack generated a power density of 0.38 W/cm^2 at 750 °C using H_2 as fuel and a multi-layered cathode composed of LSM and LSCF, and showed a long term durability of over 400 h.

The Ni-YSZ/YSZ/YSZ-LSM system has been the desired system for many researchers due to the proven long term stability of its components. For instance, using this cell configuration, Sammes et al. fabricated a 100 W modular stack using 40 single cells [13]. Ding and Liu designed a two cell stack segmented in parallel which produced 1.78 W/cm^2 at 800 °C [14]. Bai et al. made two cone shaped cells stacked in series which produced 3.7 W at 800 °C [15]. Lim et al. fabricated a stack using 30 bundles connected in series in which each bundle contained two flat tubular fuel cells connected in parallel and managed to produce 921 W at 750 °C [16]. More recently, Ye et al. fabricated a short stack using two cells connected in series and produced 5.8 W and 4.9 W power output at 850 °C in hydrogen and ethanol fuels, respectively [17]. Suzuki et al. fabricated a short stack using five fuel cells of the type Ni-GDC/GDC/GDC-LSCF which produced 2.8 V OCV and 1.5 W at 500 °C for portable applications [18].

Sarkar's research group from Alberta Innovates-Technology Futures (AITF) published several patents on stack system design during 2004–2010 [19–22]. As presented originally in [23] and shown in Fig. 2, his suggested SOFC based power generator consists of a fuel reformer, modular SOFC stacks, a catalytic combustor, air blower, a thermal recuperator and a power conditioning unit/DC to DC converter. Electrical systems and sensors monitor the whole process to ensure that the system was operating under its optimum conditions. The stack was self-sustained and an in-house designed catalytic burner provided sufficient heat to take the stack to its operating temperature. Using the catalytic combustor, no external heat source was needed. From this design, they fabricated a stack consisting of 60 anode supported μt-SOFCs [23] as shown in Fig. 3a. Humidified hydrogen and air were fed to the anode and cathode, respectively. Fuel was injected into the open end of each cell using an Inconel tube. A machined glass-ceramic was used as the cell holder and a mica gasket provided suitable sealing. A catalytic burner was embedded between the cells to start up the stack as shown in Fig. 3b. To improve the temperature uniformity inside the stack, a high emissivity foil surrounded the stack and a high emissivity coating covered the current collector surface of each cell cathode. The stack ran for 1000 h without any major problem when it faced several on/off stages. The total generated power reached 20 W which was lower than expected. This was attributed to sagging Inconel fuel inlet tubes which touched the anode surface

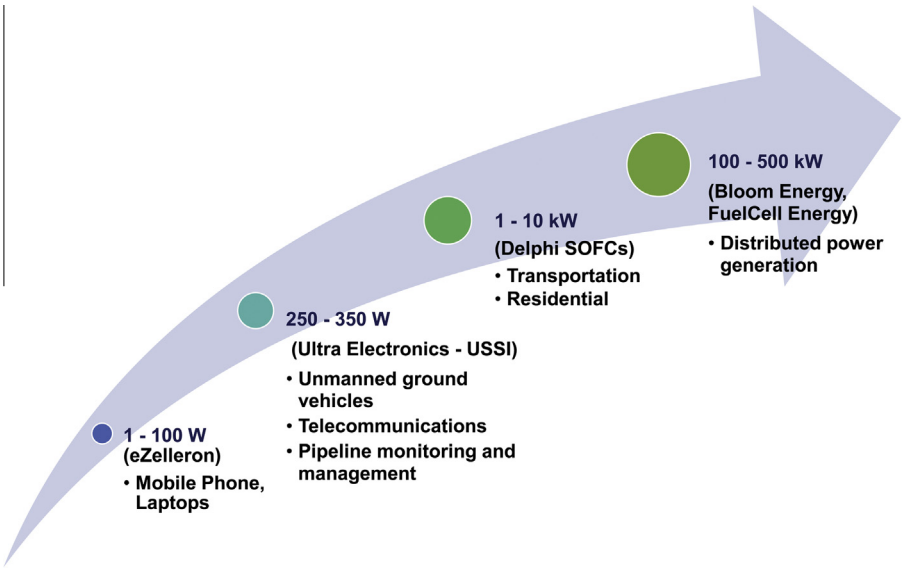

Fig. 1. Applications of SOFC stacks according to their power rating. Manufacturer names appear in parenthesis.

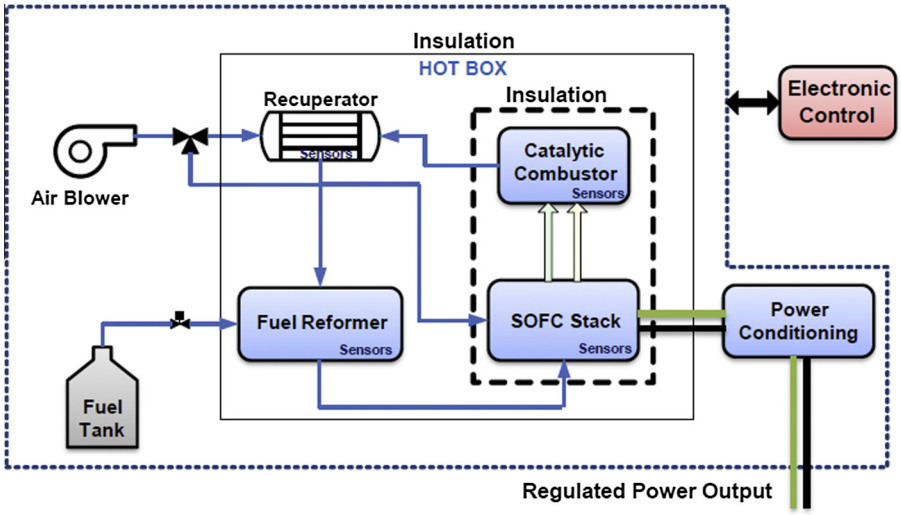

Fig. 2. Schematic of an SOFC stack and its different components, courtesy of Taylor and Francis Group [23].

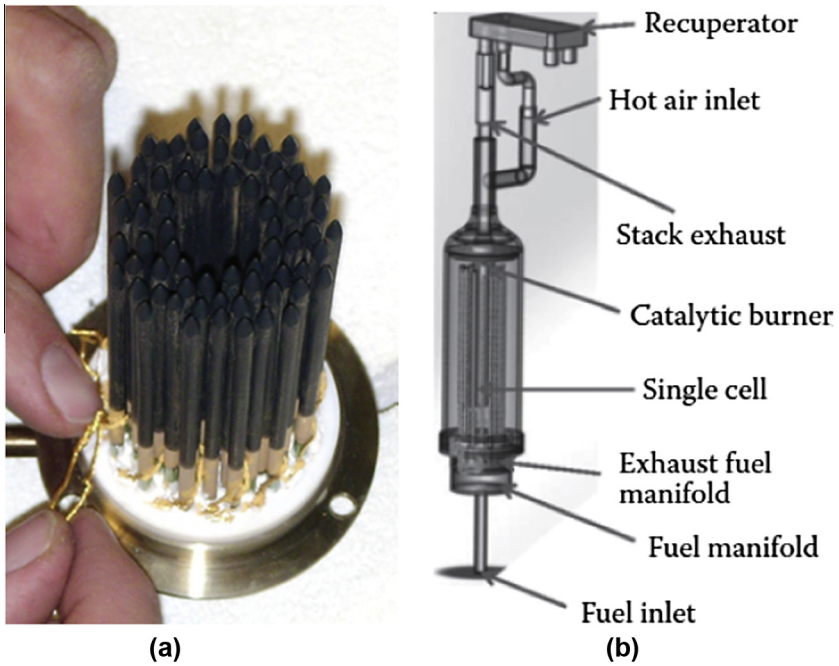

Fig. 3. Schematics of (a) the stack of 60 tubular cells, (b) catalytic burner, courtesy of Taylor and Francis Group [23].

and short-circuited the stack. Fabrication of a larger fuel cell stack using Sarkar's design is a future plan for the authors.

Reduction of the fuel cell operation temperature to intermediate temperatures (below 700 °C) improves the fuel cell life and stability, and decreases fabrication costs by utilizing common metals [24,25]. During the past couple of years, different groups have attempted to achieve high power densities at low temperatures using novel electrolyte or electrode materials [26–29]. In recent years, the nickelates ($Ln_2NiO_{4+\delta}$, with Ln = Nd, La or Pr) have been widely investigated [30–32] due to their MIEC (mixed ionic and electronic conductor) behaviour, i.e., they exhibit good electronic conductivity due to the rare earth metal mixed valence and good ionic transport due to excess oxygen [31]. Laguna-Bercero et al. [32] investigated infiltration of $Nd_2NiO_{4+\delta}$ as a cathode for anode supported tubular SOFCs, in order to avoid high temperature sintering of the nickelate phase with the electrolyte. A maximum power density of 400 mW/cm^2 was achieved at 600 °C for the Ni-YSZ/YSZ/Nd_2NiO_4-YSZ cell, and no degradation was detected after 24 h under current load.

Long term stability or, in other words, low power degradation rate is a crucial feature for commercialization of a fuel cell stack. Fig. 4 lists some of the challenges in SOFC stack development [25]. In the absence of efficient thermal management within the stack, local higher temperature gradients develop in the cells causing thermal stresses and failure of the cells. For portable applications, brittle ceramic fuel cells should show high thermal shock resistance due to rapid heating and cooling during start up and shut down. Additionally, the reduction of fabrication cost and optimization of the fuel flow manifold are other crucial aspects in SOFC commercialization and design. Minor defects in sealing can lead to fuel leakage causing not only fuel loss but also reduction in power density due to re-oxidation of the anode. Proper current collection

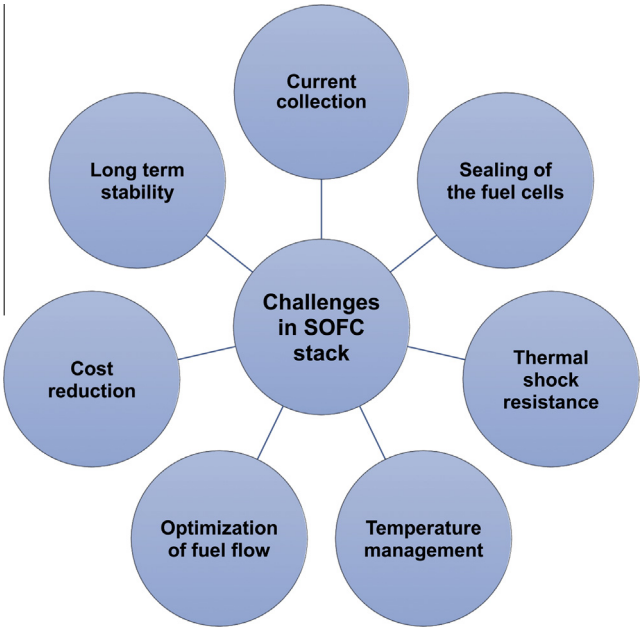

Fig. 4. Challenges in SOFC stack design and fabrication [25].

from the fuel cells is critical for achieving high power density and fuel efficiency. It is a combination of many variables including contact resistance, temperature, choice of current collection materials, geometry of the cells and the type of electrical connections. The electrical connections in an SOFC tubular stack are not well studied to date. For instance, it is not clear which arrangement (series, parallel or a mixed combination) is better in a stack in terms of power performance and reduced losses. Due to the fabrication procedure (forming and sintering) of ceramic fuel cells which involve highly brittle materials, there is always a chance of defects such as cracks in the electrode and electrolyte which lead to cell failure at operating temperatures. Cracks and defects can also form in the cells during stack assemblage. In a stack which sometimes contains hundreds of cells, it is highly possible to have defective fuel cells which in extreme cases can even lead to complete stack shut down and loss of the valuable energy conversion device. For instance, Malzbender et al. [33] found that the reason for their SOFC stack failure was weakening and fracture of the 8YSZ electrolyte along the grain boundaries due to diffusion of elemental Mn. They stated that the growth of the resulting cracks led to failure of one of the cells, direct burning of fuel gas and complete failure of the whole stack. Therefore, it is important to design the electrical connections in a way that the stack can be repaired by replacing the malfunctioning unit. A repairable fuel cell stack paves the way for commercialization of these devices by optimizing their performance and reducing valuable energy losses. These concerns were also expressed by Lawlor et al. [25] and the current study tries to find an answer to them. To the best of our knowledge the current manuscript is the sole source of information in the SOFC field about the practical advantages and disadvantages of different electrical connections in a stack, how to achieve a desired current and voltage, and how to repair a stack.

For the purpose of the current research, the short fabricated stack was simply placed in a small tubular furnace to reach to the operating temperature. The stack composed of six anode supported tubular fuel cells was tested in an intermediate temperature range of 600–700 °C. Along with $Nd_2NiO_{4+\delta}$ (NNO), the $Pr_2NiO_{4+\delta}$ (PNO) cathode was also studied due to its high oxygen diffusion parameters [34]. Fabrication and microstructural analysis of the fuel cells, along with electrochemical performance of single cells and their electrical connections in series, parallel or mixed combinations, are discussed in this study.

2. Experimental methods

2.1. Fuel cell fabrication

The tubular ceramic SOFCs investigated here were fabricated by slip casting of a NiO-YSZ anode support, followed by dip coating of a thin YSZ electrolyte and a thin porous layer for cathode infiltration. $Nd_2NiO_{4+\delta}$ or $Pr_2NiO_{4+\delta}$ were infiltrated into the thin porous YSZ layer of the cells to form the cathode.

NiO (Baker Chemicals) and YSZ (TZ-8Y, 8 mol% Y_2O_3, Tosoh) were mixed in a ratio of 65:35 wt% and milled for 72 h in a ball mill. The solid loading of the slip was set to 40% by adjusting the water content and its final pH was set to 4.0 using 2% hydrochloric acid. To generate sufficient porosity, 30 vol.% graphite (Sigma Aldrich <325 mesh) was added to the slip following pH adjustment, and then the suspension was mixed for 15 min prior to slip casting. To create the tubular support, the slip was cast into a plaster mold (previously prepared from a tubular mandrel) and left for about a minute, after which the excess slip was quickly poured out. The wet tube was then dried at room temperature for 1 h. The slip cast tubes were dried at 100 °C, then heated at 700 °C to burn off the graphite and then finally pre-sintered under air at 1000 °C for 3 h. Further details regarding the slip casting procedure and fabrication of thin tubular supports can be found in [35].

The electrolyte and the thin porous YSZ layer formulae and their dip coating procedure were previously addressed in [36,37]. Both layers were sintered at 1350 °C for 3 h. The infiltration of $Nd_2NiO_{4+\delta}$ (NNO) into a thin porous YSZ layer is addressed in [32] while the infiltration of $Pr_2NiO_{4+\delta}$ (PNO) follows a similar process.

Two of the SOFCs (C1 and C4) were infiltrated with PNO, while the remaining four (C2, C3, C5 and C6) were infiltrated with NNO. The outer diameter of the cells was about 6 mm and each cell had an active cathode area of 7.2–7.5 cm^2. A stack was fabricated that consisted of these six cells arranged in a hexagonal pattern. It was discovered that Cell C6 was broken after initial testing at 600 °C but it was incorporated into the stack at this temperature and was removed at higher temperatures.

2.2. Assembly of stack

Each single cell manifold was prepared individually and then all six cells were bundled together as a stack. Fig. 5 shows a schematic cross section of the different layers comprising the fuel cells and their testing setup. For cathode current collection, a thin coating of silver alloyed with 10 wt% Pd paste was applied on the cell cathode, wrapped with silver mesh (Alfa Aesar) and secured with two 0.58 mm diameter silver wires. A rolled copper mesh current collector (Alfa Aesar) was tightly pushed inside the tube to ensure good contact with the anode wall. Each tubular fuel cell was attached to a mullite tube using Ceramabond 552-VFG/thinner (Aremco, NY) (Fig. 5). This cement was also used for better sealing of the other end of each cell (to where the cathode was not extended). Nitrogen was fed to each tube at a rate of 50 mL/min through a stainless steel hypodermic needle. A thin stainless steel tube was also used as the anode gas outlet. The outer end of the mullite tube was sealed with wax (Fig. 5).

The fuel cell assembly (Fig. 6a) was placed in a furnace with the electrochemically active region in the hot zone. Several thermocouples continuously recorded the temperature within the testing temperature range of 600–700 °C. After heating the stack to 600 °C, reduction of the anodes was carried out, switching gradually from nitrogen to humidified hydrogen (3 vol.% H_2O) (5 mL/min change

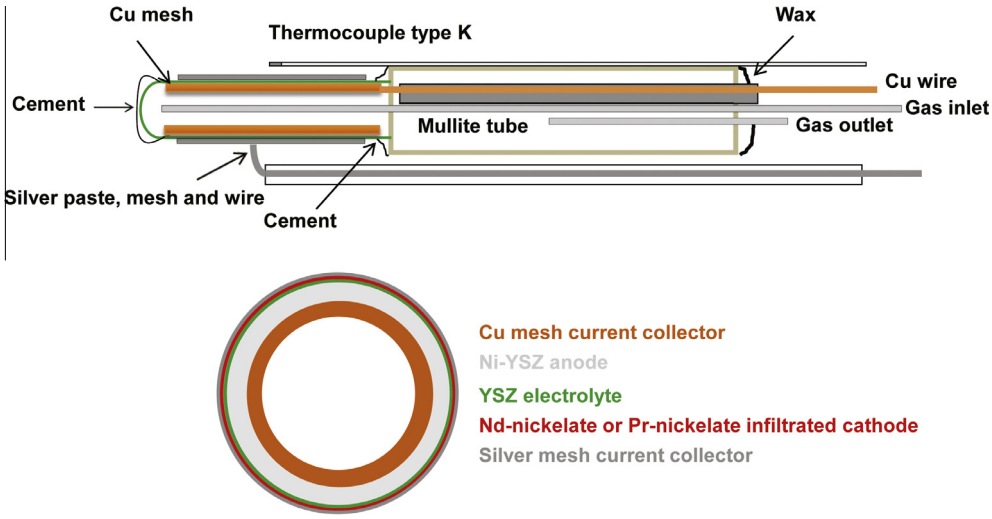

Fig. 5. Cross section of the fuel cells used in the stack and the testing set up for a single cell.

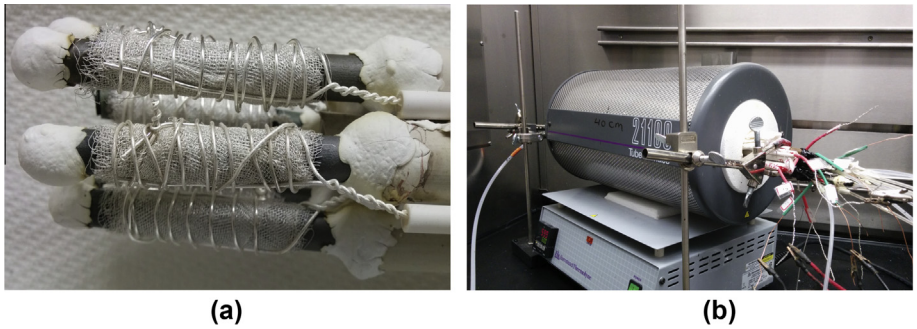

Fig. 6. (a) Tubular SOFC stack after test, (b) anode and cathode wire leads.

every 15 min maintaining the total nitrogen and hydrogen gas flow at 50 mL/min). The entire reduction process occurred over 2½ h. Air was introduced to the cathode of the cells at a similar flow rate. An Agilent electronic load (model # N3301A) evaluated the open circuit voltage (OCV) and I-V curves. An Agilent scanner (model # E4970A) monitored the thermocouples, while LabView software was used for automated measurements and data collection. AC impedance spectroscopy was carried out with a four probe configuration using a Solartron 1255 frequency response analyzer in combination with a Solartron 1287 electrochemical interface.

Each silver wire (cathode wire) was covered with a red plastic shield and each copper wire (anode wire) with a green plastic shield outside the furnace (Fig. 6b). Fig. 7 shows different electrical connections studied in this research. Each fuel cell is shown as a voltage source with an internal resistance. Using the anode and cathode wires, the cells were arranged in series and parallel configurations (Fig. 7a and b). For instance, for a parallel arrangement, the anode wires of all the fuel cells were connected to each other and their cathode wires were also connected. The two resulting thick anode and cathode wires were used for electrochemical performance testing. For a series arrangement, the anode wire of one cell was connected to the cathode of the adjacent cell in the whole bundle and the end anode and cathode wires were used for testing. Fig. 7c shows two sub-stacks of C1, C2 and C3 and of C4, C5 and C6 connected in series while the cells in each sub-stack were connected in parallel. In this manuscript this arrangement is referred to as "parallel-series". The order of the stack testing at each operation temperature was 1. Parallel, 2. Series, and 3. Parallel-series.

Following cell testing, the microstructure of the fuel cells was studied on a fractured piece by scanning electron microscopy using a Zeiss EVO MA 15 LaB6 filament scanning electron microscope.

3. Results and discussion

3.1. Structural characterization of the cells

The microstructures of two fuel cells were characterized under SEM after electrochemical performance testing. Fig. 8a and b shows part of the cross section of cells C4 and C5, respectively. The anode, electrolyte and cathode thicknesses of both cells are very similar at about 340, 15 and 30 μm, respectively. The anode of these cells showed 33% open porosity following a density test using Archimedes principle. The electrolyte appears to be dense with a minor amount of closed pores. Fig. 8c shows the needle-like structure of the PNO phase distributed on YSZ grains in cell C4. Fig. 8d shows a similar NNO phase morphology in the cathode of C5. Such morphology of the infiltrated nickelate phase has been previously reported [32]. Both phases have covered the YSZ grains well and show a suitable connectivity. Considering the weight gain of the cathode following nickelate phase infiltration into the thin porous YSZ layer, the ratio of YSZ:nickelate was calculated to be about 69:31 vol.%. This led to a 14% decrease in the total open porosity of the cathode from 50% to 36% which is still sufficient for air diffusion.

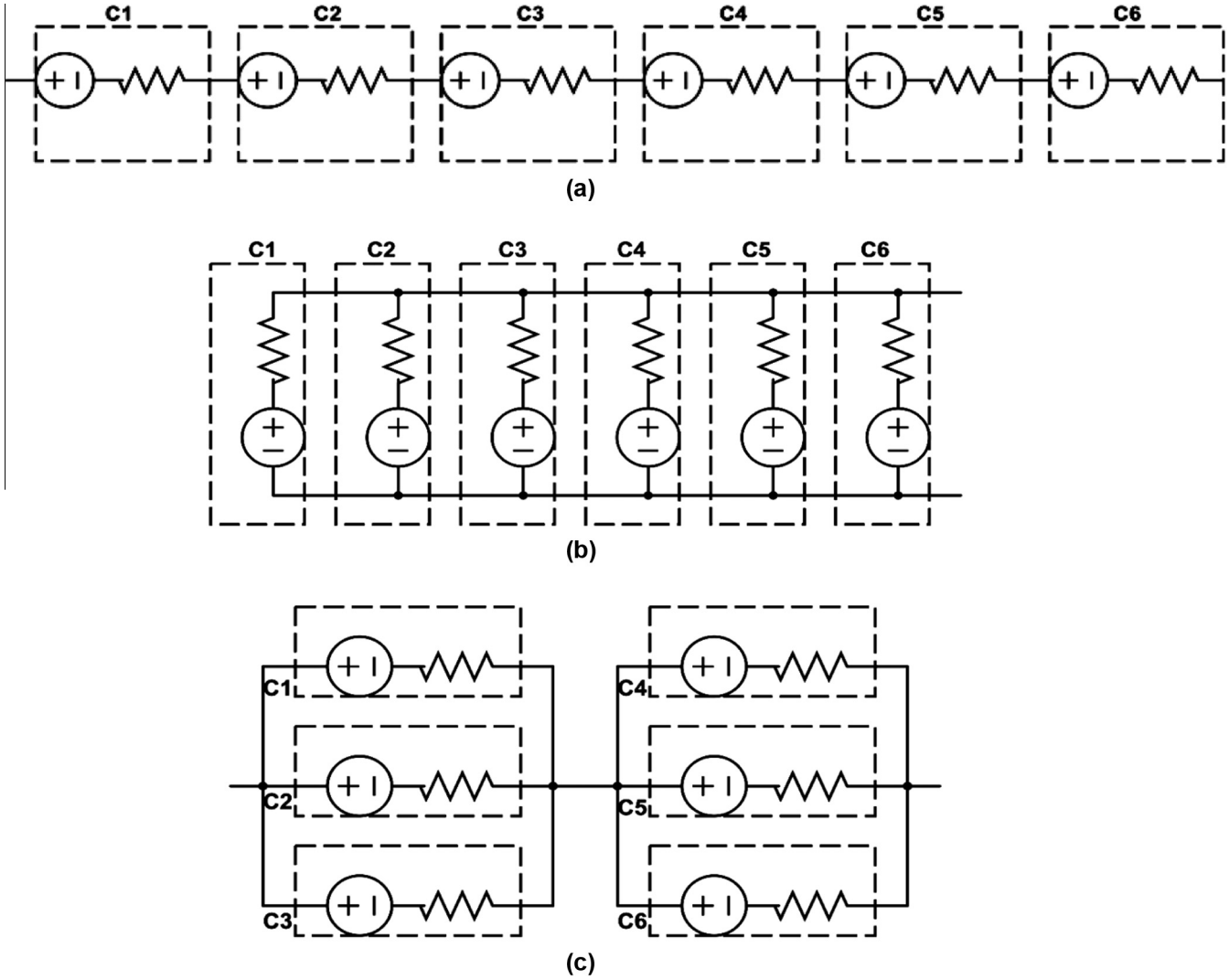

Fig. 7. Different fuel cell configurations. (a) Series, (b) Parallel and (c) Parallel-series. Cell C6 was eliminated from the tests above 600 °C due to cracking.

3.2. Single fuel cell performance

Fig. 9a–c shows I-V curves for individual cells at 600–700 °C. Table 1 summarizes the OCV and overall generated power as well as power densities of each individual cell. The OCV of the cells C1 to C5 was very similar (1.10–1.11 V) at all temperatures. The high OCV values of these cells indicate that the electrolyte became dense with no cracks formed after sintering. The OCV value of cell C6 at 600 °C (0.97 V) dropped completely to zero at 650 °C. This can be due to microcracks in the electrolyte of this cell (may have formed during cell fabrication or stack assemblage as explained in the introduction) which propagated during testing and led to complete cell failure.

At 600 °C, maximum total power of 1.48 W (202 mW/cm^2) was obtained at 0.46 V and 3.22 A for cell C1, which had PNO/YSZ as the cathode. This cell showed the best performance among all cells at the other temperatures as well (2.21 W (302 mW/cm^2) at 650 °C and 2.49 W (340 mW/cm^2) at 700 °C). In the case of NNO/YSZ cathodes, maximum power of 2.4 W (335 mW/cm^2) was recorded at 700 °C for cell C3. Overall C3 shows virtually identical power density values to C1. For cell C2, the relative performance improved with an increase of testing temperature. The maximum power increased 2.5 fold with a temperature increase from 600 to 700 °C, in comparison to a 68% increase for cell C1. Overall, the performance of C2 conformed to the performance of the other cells at higher temperatures. At all three temperatures, the performance of C1 and C4 is within ±5%, indicating that cell performance was reproducible. For NNO/YSZ cathode cells (C3 and C5), the performance showed similar behaviour and cell C2 conforms to them at higher temperatures. Cell C6 delivered 0.43 W (57 mW/cm^2) at 600 °C which was significantly lower than other cells. Generally, it can be said that the cells containing PNO or NNO cathodes show similar power outputs.

Fig. 10a and b shows the ac impedance spectra of cells C4 and C5 within the temperature range of 600–700 °C. An equivalent circuit model is also shown in this Fig. 10(c) which includes the ohmic resistance (R_s) and the non-ohmic polarizations (R1 and R2) of the tubular cells. For comparison, the ohmic resistance, non-ohmic polarizations and the total polarization of these cells based on the fit data are summarized in Table 2.

Analyzing the impedance spectra, it is seen that the polarization spectra consist of two semicircles: one in the high-medium frequency range (>10 Hz) and one in the low frequency range (<10 Hz). The former semicircle is larger than the latter one. It has been previously shown that the high-medium frequency semicircle is related to charge transfer resistance corresponding to electron-ion transfer processes occurring at the interfaces and also non-charge transfer processes corresponding to surface reactions,

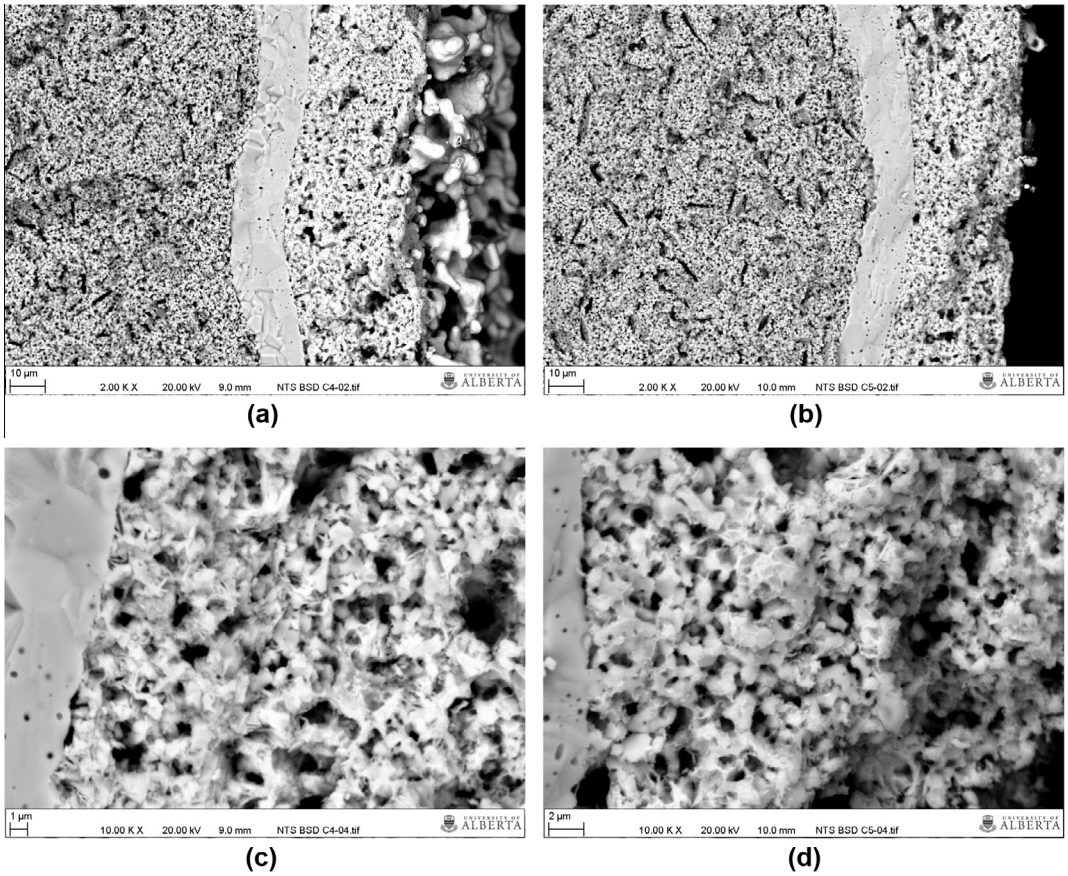

Fig. 8. SEM images of cells C4 and C5 following testing. (a) Interface of anode (left), electrolyte and cathode (right) in C4, (b) interface of anode (left), electrolyte and cathode (right) in C5, (c) cathode of C4: $Nd_2NiO_{4+\delta}$ infiltrated into porous YSZ, (d) cathode of C5: $Pr_2NiO_{4+\delta}$ infiltrated into porous YSZ.

while the low frequency semicircle is attributed to mass transfer processes [38–40]. It can be seen that both cells show relatively similar ohmic resistance. Both activation and concentration polarization are smaller for cell C5 at all temperatures which can be the reason for the slightly improved power density of this cell compared with C4. This means that cell C5 is electrochemically more active and its anode microstructure shows less resistance towards gas diffusion. The recorded ohmic resistances are higher than the planar design due to the longer current path in tubular cells which is the main reason for lower power performance of tubular cells.

3.3. Performance of SOFC stack under different arrangements

Fig. 11a–c and Table 3 show the performance of the stack under different electrical connections tested at 600–700 °C. OCV of the stack under parallel arrangement was 1.10 V despite the broken C6, possibly due to the dominance of the stack voltage by the presence of five cells showing OCV of 1.10 V. Under the series arrangement, OCV changed to 5.50 V and not zero indicating that the OCV of C6 had not dropped to zero at this stage. It was expected to reach to a power of zero under the series arrangement over time when cell C6 became completely non-functional. Under the parallel-series arrangement, the recorded OCV was 2.13 V which is lower than 2.20 V calculated assuming all cells showed OCV of 1.10 V. This drop in OCV is clearly due to the broken cell in the second sub-stack. The testing continued at 600 °C with the malfunctioning fuel cell. The presence of such a cell provides a better insight into a realistic stack performance, as in a large stack there is a high probability that individual fuel cells may become defective during fabrication or stack assemblage. The order of power performance at 600 °C was observed to be parallel (7.40 W) > parallel-series (7.37 W) > series (6.52 W). This indicates that the stack power under the series arrangement was more negatively impacted due to the broken C6. As shown in Fig. 11a, under series mode the highest voltages (5.5–0.3 V) and the lowest currents (0–5 A) were derived from the stack. However, under parallel mode the lowest voltages (1.1–0.3 V) and highest currents (0–20 A) were recorded. Parallel-series showed intermediate voltage (2.1–0.3 V) and current (0–11 A) values and similar current-voltage correlations.

It is important to mention that for an ideal arrangement, the total power measured should be equal to the sum of the power generated by individual cells, for instance at 600 °C, i.e., 7.17 W. This is lower than the actual power measured for the parallel and parallel-series arrangements. One possible reason for this observation might be the performance of cell C2. It is assumed that the cell was not fully reduced during individual cell testing, which adversely affected its performance. Due to the nature of the ceramic fuel cells' microstructure which can differ slightly from one cell to another, the gas diffusion and overall reduction process might be slower in some fuel cells. Normally, a cell shows its highest performance when it is completely reduced and the nickel phase catalyses the electrochemical reactions and provides the electrical current path. As observed in Fig. 9 and Table 1, the improvement in performance of cell C2 with increase in temperature was more significant than other cells. Different electrical connections testing of the stack was performed a few hours following single cell testing which can be the reason for full reduction and stabilization of cell C2, and its better performance and contribution to stack performance.

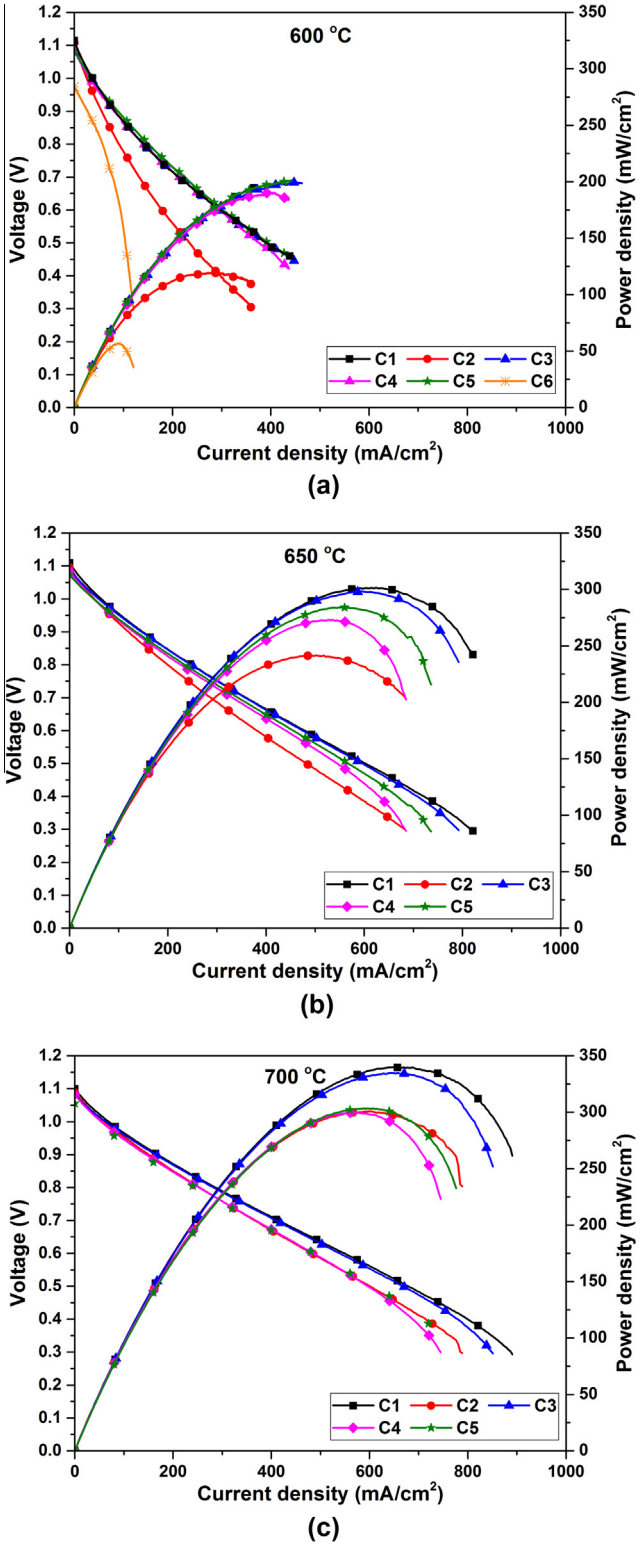

Fig. 9. Individual fuel cell performance under humid hydrogen at (a) 600 °C, (b) 650 °C and (c) 700 °C.

When the electrical power of the fuel cells in a stack are not matched, this leads to rapid performance degradation. Any weak fuel cell in a stack connected in series needs to work hard in order to pass the same current as the higher performing fuel cells which causes a quicker degradation. Such a cell degrades to a point that it becomes non-functional and an additional load for the stack. Such an increased load on the other fuel cells leads to a higher degradation rate and eventually stack failure. Therefore, the weakest cell determines the stack power [24]. In the case of designing a stack based on a modular design (mixed series and parallel), it is possible to remove the damaged section of the stack and replace it with new cells so the stack can operate at its maximum capacity. Therefore, cell C6 was removed from the stack during testing at temperatures above 600 °C to not adversely affect its performance.

As shown in Fig. 11b and Table 3, the maximum power at 650 °C was recorded for the parallel arrangement (10.32 W), equal to the sum of individual cell powers at 650 °C (10.31 W). The performance of series and parallel-series arrangements were quite similar. Fig. 11c shows the performance of different arrangements at 700 °C. Both series (11.56 W) and parallel (11.40 W) designs delivered powers close to the sum of individual cell performances (11.65 W) at this temperature and showed a higher power than the parallel-series mode. However, the stack under different electrical arrangements does not show significant differences in power. Similar to 600 °C, at higher temperatures the series mode shows the highest voltage and least current while the parallel mode shows the reverse behaviour. As for 600° and 650 °C, the parallel-series mode shows intermediate currents and voltages.

Fuel cells connected in series maintain the same current and increase the stack voltage and, as discussed, the current is controlled by the worse performing cell. On the other hand, cells connected in parallel maintain the same voltage and increase the total current. A high resistance cell in a parallel connection is less critical than a series arrangement but naturally reduces the total load capability. However, due to more wires needed in a parallel design, there are more associated losses and the materials cost in the stack increases [24,25]. In addition, under the parallel arrangement, power loss is greater in the tubular design compared with the planar design due to the longer current path. The low voltage delivered in a parallel design makes the voltage conversion also difficult for the interface voltage convertors. As discussed in this study, the parallel-series configuration not only offers similar power performance compared to that of series or parallel configurations but also allows the stack to run under an intermediate voltage and current which can be more advantageous for operation as well as in terms of current collector costs.

A stack can also be fabricated based on a series-parallel configuration where modules are connected in parallel while the cells within each module are connected in series. This arrangement will offer higher voltage but lower current compared with parallel-series mode. The choice of series-parallel or parallel-series depends on the application and the required voltage and current. The cell arrangement can be designed by incorporating a suitable number of single cells in each module. Such arrangements are more practical to use in case any fuel cell malfunctions during operation since the damaged module can be replaced by new cells without affecting the entire stack performance. This is the benefit that especially cannot be enjoyed in a series configuration.

4. Conclusions

In this research the incorporation of high performing nickelate cathodes into a fuel cell stack was evaluated. Nd-nickelate and Pr-nickelate cathode performances were studied in the 600–700 °C temperature range. No significant difference was observed in the performance with the power generation being within a 10% range. Overall, individual cell performances were in good conformity with each other making the results reproducible. The stack was tested under different electrical connections for which similar powers were derived. Incorporation of a malfunctioning fuel cell into the stack at 600 °C affected the power and OCV of the series

Table 1
Open circuit voltage (OCV) and generated power of the individual stack fuel cells.

Temperature (°C)	Fuel cell	OCV (V)	Peak power density (mW/cm^2)	Total power (W)
600	C1	1.11	202	1.48
	C2	1.11	120	0.89
	C3	1.10	200	1.43
	C4	1.10	191	1.43
	C5	1.10	201	1.51
	C6	0.97	57	0.43
650	C1	1.11	302	2.21
	C2	1.10	242	1.80
	C3	1.10	298	2.13
	C4	1.10	273	2.04
	C5	1.10	284	2.13
700	C1	1.10	340	2.49
	C2	1.10	301	2.23
	C3	1.10	335	2.40
	C4	1.10	300	2.25
	C5	1.10	304	2.28

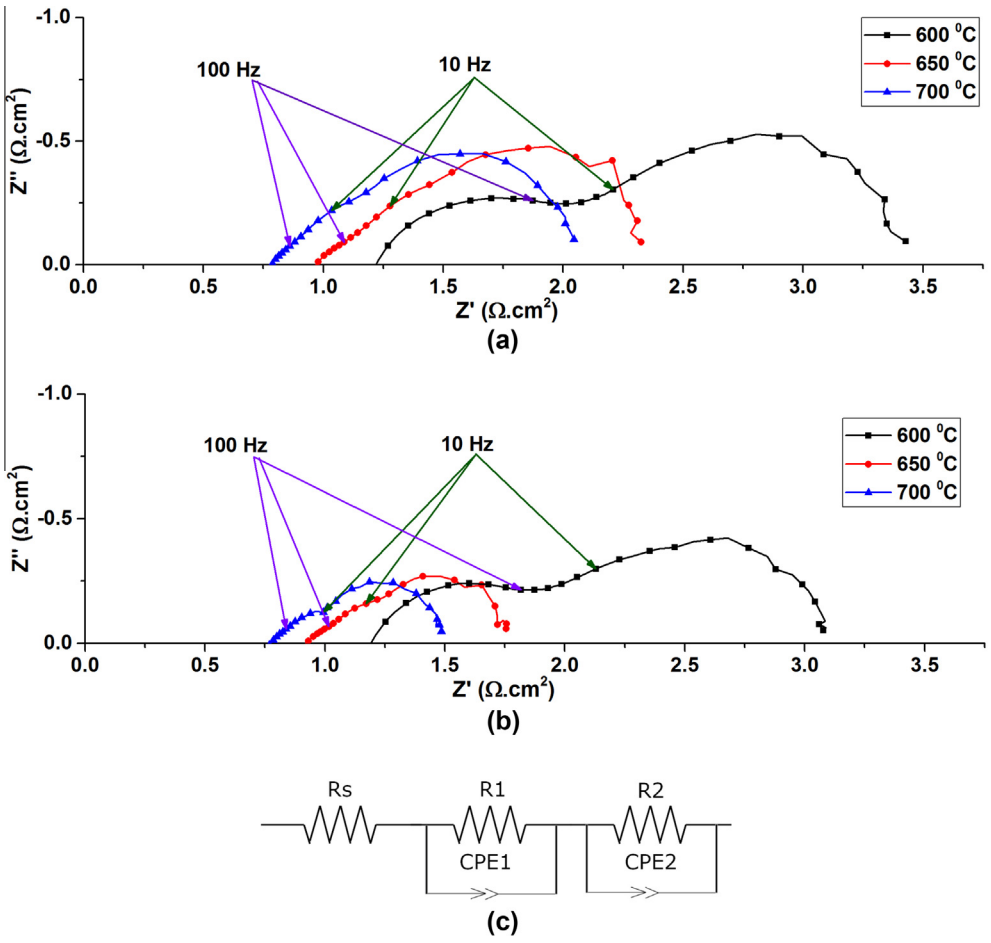

Fig. 10. Impedance spectra of (a) C4 and (b) C5, and (c) equivalent circuit model.

Table 2
Ohmic and polarization resistances of cells C4 and C5.

Temperature (°C)	Fuel cell	R_s (Ω cm^2)	R_1 (Ω cm^2)	R_2 (Ω cm^2)	ASR (Ω cm^2)
600	C4	1.24	0.83	1.42	3.49
	C5	1.19	0.74	1.21	3.14
650	C4	0.97	0.75	0.68	2.40
	C5	0.93	0.59	0.27	1.79
700	C4	0.78	0.75	0.55	2.08
	C5	0.77	0.35	0.37	1.49

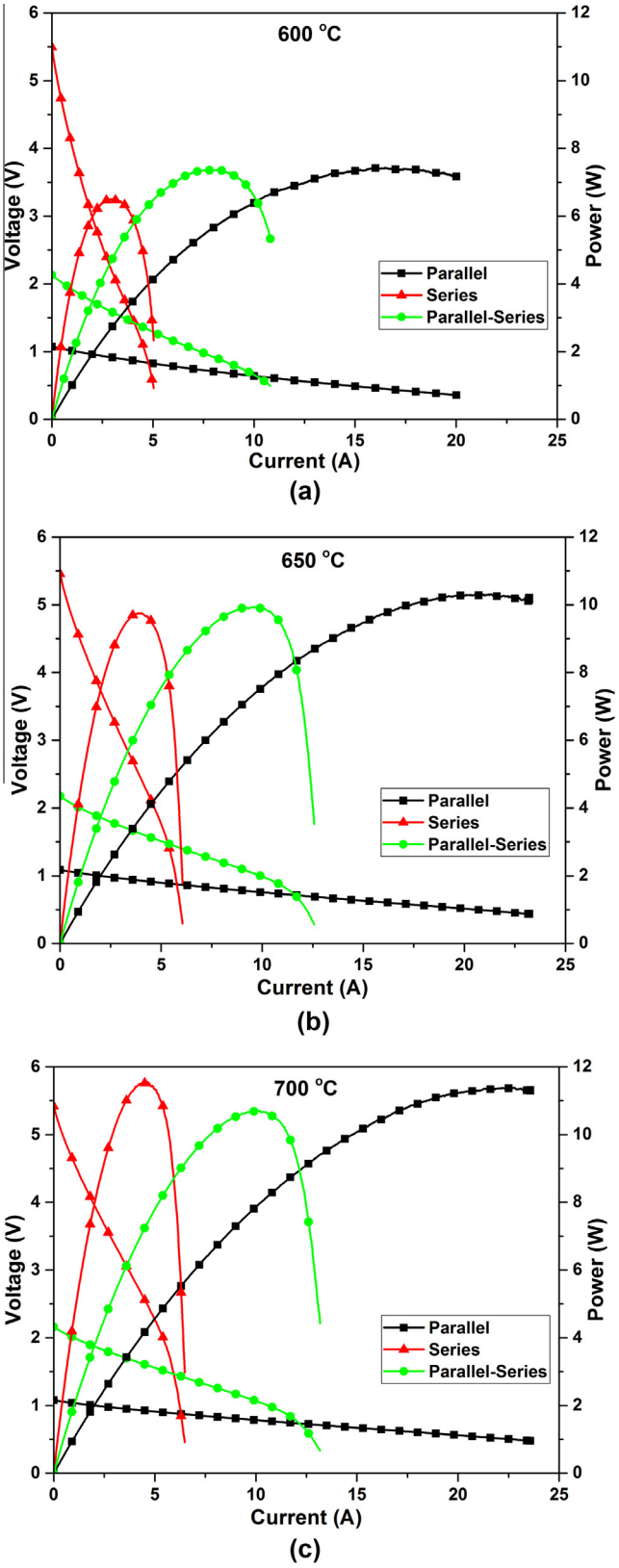

Fig. 11. Electrochemical performance of the stack under different electrical arrangements at (a) 600 °C, (b) 650 °C and (c) 700 °C.

arrangement the most and the parallel arrangement the least. Using mixed series and parallel combinations not only offers a high current or voltage and similar power performance, but also is safer to run in case any cell fails during operation. A stack with the cells connected under a mixed arrangement can be repaired in case a cell in a module fails by replacement of the corresponding module. The repairability is vital for commercialization of fuel cell stacks by preserving the energy conversion device which can be feasible by proper selection of electrical connections among the fuel cells.

Table 3
Open circuit voltage and total power of the stack under different electrical connections.

Temperature (°C)	Arrangement	OCV (V)	Total power (W)
600	Parallel	1.10	7.40
	Series	5.50	6.52
	Parallel-series	2.13	7.37
650	Parallel	1.10	10.32
	Series	5.50	9.76
	Parallel-series	2.17	9.94
700	Parallel	1.10	11.40
	Series	5.42	11.56
	Parallel-series	2.16	10.70

Acknowledgement

The authors would like to acknowledge the Climate Change and Emissions Management Corporation (CCEMC) of Canada for funding this research.

References

[1] Minh NQ. Ceramic fuel-cells. J Am Ceram Soc 1993;76:563–88.
[2] Stambouli AB, Traversa E. Fuel cells, an alternative to standard sources of energy. Renew Sustain Energy Rev 2002;6:295–304.
[3] Choudhury A, Chandra H, Arora A. Application of solid oxide fuel cell technology for power generation – a review. Renew Sustain Energy Rev 2013;20:430–42.
[4] Jamil SM, Othman MHD, Rahman MA, Jaafar J, Ismail AF, Li K. Recent fabrication techniques for micro-tubular solid oxide fuel cell support: a review. J Eur Ceram Soc 2015;35:1–22.
[5] Lee SB, Yun KS, Lim TH, Song RH, Shin DR. Development of anode supported micro-tubular SOFC stack for APU application. In: Eguchi K, Singhai SC, Yokokawa H, Mizusaki H, editors. Solid oxide fuel cells. p. 187–91.
[6] Kendall K. Progress in microtubular solid oxide fuel cells. Int J Appl Ceram Technol 2010;7:1–9.
[7] Sarkar P, Yamarte L, Rho HS, Johanson L. Anode-supported tubular micro-solid oxide fuel cell. Int J Appl Ceram Technol 2007;4:103–8.
[8] Cheekatamarla PK, Finnerty CM, Robinson CR, Andrews SM, Brodie JA, Lu Y, et al. Design, integration and demonstration of a 50 W JP8/kerosene fueled portable SOFC power generator. J Power Sourc 2009;193:797–803.
[9] Torrell M, Morata A, Kayser P, Kendall M, Kendall K, Tarancon A. Performance and long term degradation of 7 W micro-tubular solid oxide fuel cells for portable applications. J Power Sourc 2015;285:439–48.
[10] Du Y, Finnerty C, Jiang J. Thermal stability of portable microtubular SOFCs and stacks. J Electrochem Soc 2008;155:B972–7.
[11] Singhal SC, Kendall K. High temperature solid oxide fuel cells: fundamentals, design, and applications. 1st ed. Oxford: Elsevier; 2003. p. 61.
[12] Alston T, Kendall K, Palin M, Prica M, Windibank P. A 1000-cell SOFC reactor for domestic cogeneration. J Power Sourc 1998;71:271–4.
[13] Sammes NM, Du Y, Bove R. Design and fabrication of a 100 W anode supported micro-tubular SOFC stack. J Power Sourc 2005;145:428–34.
[14] Ding J, Liu J. A novel design and performance of cone-shaped tubular anode-supported segmented-in-series solid oxide fuel cell stack. J Power Sourc 2009;193:769–73.
[15] Bai Y, Liu J, Wang C. Performance of cone-shaped tubular anode-supported segmented-in-series solid oxide fuel cell stack fabricated by dip coating technique. Int J Hydrogen Energy 2009;34:7311–5.
[16] Lim TH, Park JL, Lee SB, Park SJ, Song RH, Shin DR. Fabrication and operation of a 1 kW class anode-supported flat tubular SOFC stack. Int J Hydrogen Energy 2010;35:9687–92.
[17] Ye XF, Yuan C, Chen YP, Zhong CY, Zhan ZL, Wang SR. Micro-tubular solid oxide fuel cells and their stacks running on direct ethanol fuels. J Electrochem Soc 2014;161:F894–8.
[18] Suzuki T, Funahashi Y, Yamaguchi T, Fujishiro Y, Awano M. Development of cube-type SOFC stacks using anode-supported tubular cells. J Power Sourc 2008;175:68–74.
[19] Sarkar P, RhO H. Tubular solid oxide fuel cell stack. In: Patent U, editor. US Patent. USA; 2004.
[20] Sarkar P, Rho H, Johanson L. Solid oxide fuel cell system. In: Patent U, editor. USA; 2005.
[21] Zheng R, Rho H, Yamarte L, Kovacik G, Sarkar P. Controlling solid oxide fuel cell operation. In: Patent U, editor. USA; 2007.

[22] Zheng R, Kovacik G, Rho H, Sarkar P, Yamarte L, Richardson M. Heating solid oxide for fuel cell; 2010.
[23] Sarkar P, Amiri S. Advances in micro solid oxide fuel cells. In: Jiang SP, Shen PK, editors. Nanostructured and advanced materials for fuel cells. CRC Press; 2013. p. 69–125.
[24] Howe KS, Thompson GJ, Kendall K. Micro-tubular solid oxide fuel cells and stacks. J Power Sourc 2011;196:1677–86.
[25] Lawlor V, Griesser S, Buchinger G, Olabi AG, Cordiner S, Meissner D. Review of the micro-tubular solid oxide fuel cell Part I. Stack design issues and research activities. J Power Sourc 2009;193:387–99.
[26] Chen D, Ran R, Zhang K, Wang J, Shao Z. Intermediate-temperature electrochemical performance of a polycrystalline $PrBaCo_2O_{5+\delta}$ cathode on samarium-doped ceria electrolyte. J Power Sourc 2009;188:96–105.
[27] Dutta A, Mukhopadhyay J, Basu RN. Combustion synthesis and characterization of LSCF-based materials as cathode of intermediate temperature solid oxide fuel cells. J Eur Ceram Soc 2009;29:2003–11.
[28] Bozza F, Polini R, Traversa E. High performance anode-supported intermediate temperature solid oxide fuel cells (IT-SOFCs) with $La_{0.8}Sr_{0.2}Ga_{0.8}Mg_{0.2}O_{3-\delta}$ electrolyte films prepared by electrophoretic deposition. Electrochem Commun 2009;11:1680–3.
[29] Zhen YD, Tok AIY, Jiang SP, Boey FYC. Fabrication and performance of gadolinia-doped ceria-based intermediate-temperature solid oxide fuel cells. J Power Sourc 2008;178:69–74.
[30] Tarancon A, Burriel M, Santiso J, Skinner SJ, Kilner JA. Advances in layered oxide cathodes for intermediate temperature solid oxide fuel cells. J Mater Chem 2010;20:3799–813.
[31] Skinner SJ, Kilner JA. Oxygen diffusion and surface exchange in $La_{2-x}Sr_xNiO_{4+\delta}$. Solid State Ionics 2000;135:709–12.
[32] Laguna-Bercero MA, Hanifi AR, Monzon H, Cunningham J, Etsell TH, Sarkar P. High performance of microtubular solid oxide fuel cells using $Nd_2NiO_{4+\delta}$ based composite cathodes. J Chem A 2014;2:9764–70.
[33] Malzbender J, Batfalsky P, Vaßen R, Shemet V, Tietz F. Component interactions after long-term operation of an SOFC stack with LSM cathode. J Power Sourc 2012;201:196–203.
[34] Boehm E, Bassat JM, Dordor P, Mauvy F, Grenier JC, Stevens P. Oxygen diffusion and transport properties in non-stoichiometric $Ln_{2-x}NiO_{4+\delta}$ oxides. Solid State Ionics 2005;176:2717–25.
[35] Hanifi AR, Laguna-Bercero MA, Etsell TH, Sarkar P. The effect of electrode infiltration on the performance of tubular solid oxide fuel cells under electrolysis and fuel cell modes. Int J Hydrogen Energy 2014;39:8002–8.
[36] Hanifi AR, Paulson S, Torabi A, Shinbine A, Tucker MC, Birss V, et al. Slip-cast and hot-solution infiltrated porous yttria stabilized zirconia (YSZ) supported tubular fuel cells. J Power Sourc 2014;266:121–31.
[37] Hanifi AR, Torabi A, Chen X, Hill S, Sarkar P, Etsell TH. Development of redox resistant fully infiltrated tubular SOFCs. J Electrochem Soc 2014;161:F391–7.
[38] Adler SB. Mechanism and kinetics of oxygen reduction on porous $La_{1-x}Sr_xCoO_{3-\delta}$ electrodes. Solid State Ionics 1998;111:125–34.
[39] Reitz TL, Xiao H. Characterization of electrolyte-electrode interlayers in thin film solid oxide fuel cells. J Power Sourc 2006;161:437–43.
[40] Xin XS, Lu Z, Huang XQ, Sha XQ, Zhang YH, Chen KF, et al. Solid oxide fuel cells with dense yttria-stabilized zirconia electrolyte membranes fabricated by a dry pressing process. J Power Sourc 2006;160:1221–4.